ELSEVIER

Polymer 43 (2002) 7101–7109

polymer

www.elsevier.com/locate/polymer

Real time SANS study on head group self-assembly for lithium based anionic polymerizations

J. Stellbrink[a], J. Allgaier[a], L. Willner[a], D. Richter[a], T. Slawecki[b], L.J. Fetters[c,*]

[a]*Institute for Solid State Research, Research Center, Jülich, 52425 Jülich, Germany*
[b]*Center for Neutron Research, National Institute of Science and Technology, Gaithersburg, MD 20899-8562, USA*
[c]*School of Chemical and Biomolecular Engineering, Cornell University, Ithaca, NY 14583-5201, USA*

Received 16 November 2001; received in revised form 22 April 2002; accepted 21 May 2002

Abstract

Small angle neutron scattering was used to in situ study the aggregated structures formed in the course of the polymerization of butadiene and isoprene in deuterated *n*-heptane. The samples were designed to have equal degrees of polymerization. These measurements showed, at low Q, that the start of the butadiene propagation event was accompanied by the presence of highly extended large-scale structures. As propagation progressed these initial structures diminished in size and were replaced, at least in part, by star-like aggregates. At the cessation of the polymerization reaction the star micelles, mid-Q regime, exhibited a mean aggregation state of 8.4. At lower conversions (and thus lower chain molecular weights) the presence of large three-dimensional aggregates was indicated. Conversely, the isoprene system in its initial moments of propagation did not show the same extent of large-scale structures although the low Q data did indicate the formation of architectures larger than the star-like aggregates. The star shaped micelles exhibited the mean degree of aggregation of 4. These results demonstrate that the association behavior of these polar dienyllithium headgroups is more varied than permitted by the current 'textbook' mechanism where the solitary permissible aggregation state is four. These findings concur with those suggested from a recent semi-empirical and ab initio quantum chemistry based series of calculations.

Keywords: Self-assembly; Polymer; Headgroups

1. Introduction

The self-assembly of lithium bearing diene headgroups in anionic polymerizations conducted in hydrocarbons is recognized to lead to micellar aggregates of different architectures, i.e. linear, star shaped and cylindrical [1–4]. Similar behavior has been recorded for polyisoprene chains capped with zwitterionic headgroups in dilute solution and the melt [5–7]. Evidence for both star-like micelles and string-like structures was found. The mean aggregation numbers decreased with increasing chain length due to the repulsive excluded volume interactions among the polymeric tails. In many ways these two model ionomer structures resemble surfactants in that the semi-telechelic hydrocarbon chain is tipped with a highly polar headgroup, which is insoluble in hydrocarbon milieu (Table 1).

Polymer brush behavior [8] also plays a role in the control of the existing aggregated structures. Recently, numerical solutions of self-consistent mean-field equations were used to calculate the stretching energies of the polymer chains in micelles formed by the clustering of the lithium based allylic headgroups [9]. This exercise was accompanied by the application of semi-empirical and ab initio quantum chemistry methods to calculate headgroup geometries and binding energies. These quantum chemical calculations indicate that at low degrees of polymerization polydisperse exponentially distributed cylinder-like structure form and are, in turn, built from the dimer aggregate. The dimer structure is taken as the 'mother' aggregate. However, as chain length increases a crossover to star shaped aggregates will occur. Coexistence of both architectures is possible over a limited range of chain lengths. This behavior is prompted by the balance between the enthalpy of the aggregation events and the entropic loss occasioned by the formation of aggregates. This includes the loss of chain translational freedom, the loss of configurational entropy caused by the resulting stretching of the tethered chains and the entropic loss encountered

* Corresponding author.

0032-3861/02/$ - see front matter
PII: S0032-3861(02)00450-0

when star shaped polymers (with functionalities larger than about four) form more ordered structures in solution near the regime of the overlap concentration [10–14].

The textbook view [15–18][1] of these systems asserts that the aggregation state of the polar headgroups is directly discernible from the kinetic order exhibited by the propagation event and that only the momentarily dissociated singlet headgroup is capable of reacting with monomer. Although the 1/4 order has long endured [15–17] as the experimental kinetic order for diene polymerizations an evaluation [1] of the existing data shows that the predominant linear gradient is 1/5. All told, gradients ranging from ~1/2 to ~1/9 have been reported. As a counter point variable gradient behavior (~16 to ~1) is found in the conventional log–log plot of R_p/M vs. active center concentration. Thus, the strict correspondence between the aggregation state of four and the inverse of the kinetic order is tenuous at best for the diene systems. A small angle neutron scattering (SANS) evaluation [3] of the aggregation states of the butadienyllithium headgroup has shown that this active center can self-assemble into a much wider variety of aggregation states than is indicated by the accepted kinetic order of 1/4. Makowski and Lynn [19][2] demonstrated the existence of a wide diversity of aggregation states for oligomeric butadienyllithium in the melt-state in 1966.

This study reports on the in situ and real time SANS measurements made on polymerizing butadiene and isoprene in deuterated *n*-heptane. The data captured immediately after the completion of the initiation step show the presence of large-scale structures. These large-scale aggregates 'melt' as conversion increases.

2. Experimental

2.1. Sample preparation and characterization

The basic procedures used for the purification of solvent and monomers are described elsewhere [20]. The polymerization solvent was deuterated *n*-heptane (Chemotrade, 99.2% d) while the initiator was *sec*-butyllithium. This initiator was synthesized in *n*-pentane in our laboratory and kept until use at −25 °C. There was no evidence for the presence of non-carbon bonded lithium species in the initiator solution. Care must be exercised regarding *sec*-butyllithium since it is known to be unstable if kept at room temperature [21]. The heptane was purified by storing on the vacuum line with the adduct of diphenylethylene and *n*-butyllithium.

Table 1
Characteristics of polymer solutions

Sample	T (°C)	Conc. (g/cm^3)	Φ^a	N_0 (cm^{-3})	N_{ini} (mol/cm^3)
Butadiene	22	3.48×10^{-2}	3.87×10^{-2}	3.88×10^{2}	1.24×10^{-3}
Isoprene	22	3.55×10^{-2}	3.95×10^{-2}	3.15×10^{2}	1.02×10^{-3}

[a] Solution concentration divided by polymer density.

The cuvettes containing the solvent and solvent/monomer mixture were prepared independently on the vacuum line using the same solvent and monomer sources as were used for the solutions in the reactors, Fig. 1. These cells were used to establish the background scattering behavior, which were subsequently subtracted from the data involving the polymerizing systems. Fig. 1 shows the reactor with the various quartz cells in place. This allowed the sequential capture of cells containing solvent and initiator and solvent/initiator/monomer mixture. Two sample cells were filled with the latter solution with one serving as a spare.

The ampoules containing the initiator, monomer and CD_3OD were attached to the reactor arms that are seen in Fig. 1. For the in situ measurements the polymerizations were conducted at 22 °C and used both butadiene and isoprene monomers. The monomer concentration used for

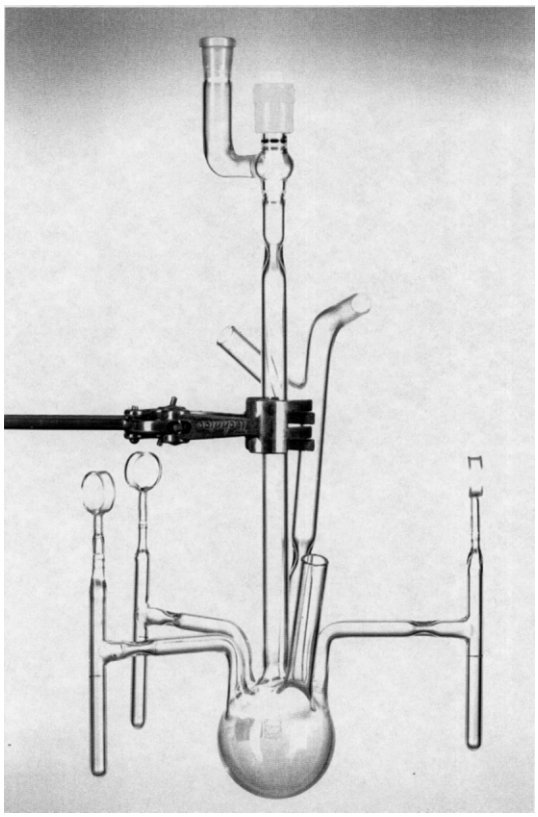

Fig. 1. Photograph of the polymerization reactor.

[1] For example, Ref. [18] states that one obtains the aggregation degree directly from the slope of the resulting straight line of the double logarithmic plot.

[2] An indication of the aggregation scale that these headgroups can form in the melt state is seen in the viscosity ratio of aggregate/singlet species. This ratio is ca. 6×10^3 when the polymerization degree of the chain in the aggregate is about 6. This ratio commences to decrease as chain length increases. The minimum degree of association available from this data is the dimer; see Ref. [19] and fig. 8 in Ref. [3].

Table 2
Characterization of terminated chains

Sample	M_n (g/mol)[a]	M_w (g/mol)[b]	M_w/M_n[b]	M_w/M_n[c]	D_p	R_g (Å)[d]	A_2 (cm^3 mol/g^2)[d]
Poly(butadiene)	25.9K	28.0K	1.03	1.08	519	70.3 ± 0.2	$3.2(\pm 0.02) \times 10^{-4}$
Poly(isoprene)	31.7K	34.8K	1.03	1.10	512	71.8 ± 0.3	$7.4(\pm 0.03) \times 10^{-4}$

[a] Membrane osmometry.
[b] SEC.
[c] SEC/membrane osmometry.
[d] SANS.

the butadiene system was 0.64 mol/l while that of the isoprene system was 0.52 mol/l. Thus the final polymer concentration (in terms of volume fraction) for both systems was ~3.9%. The headgroup concentrations N_i were ca. 1×10^{-3} mol/l. The resultant polymers had, within experimental error, identical degrees of polymerization, see Table 2.

The polymerization protocol first involved the addition of the initiator solution to the reactor followed by the removal of the hydrogenous pentane via distillation. This step was followed by the addition of the *d*-heptane. A portion of this solution was then captured in a quartz cell and the reactor and cell reservoir cooled to about −80 °C and the cell unit removed from the reactor via heat sealing at the constriction. The reactor was then returned to the vacuum line.

The required amount of monomer was then distilled into the reactor, which was then removed from the vacuum line by heat sealing at the constriction below the stopcock. The removal of these cells containing monomer/initiator/solvent solution was the same as used for the heptane/*sec*-butyllithium system. These solutions were kept at −80 °C until the SANS measurements commenced. The remaining reactor contents were then polymerized at 20 °C. The temperature of the SANS measurements (22 °C) was chosen so as to yield a convenient polymerization rate. To this end the diene propagation rate data of Sinn and coworkers [22,23] were useful.

Distilling in degassed *d*-methanol into the reactor terminated the final polymerized product. These solutions were filtered to remove the lithium methoxide. A portion of each solution was placed in a quartz cell and thus served as the terminated sample for each polymer system. The polybutadiene and polyisoprene samples were then isolated, dried and characterized via on-line SEC-light scattering. THF was the carrier solvent at 30 °C. Fig. 2 shows the SEC traces of these polymers and the characterization findings. These results were identical to those obtained from the polymers obtained from the cuvettes following the SANS measurements. These latter evaluations were done using a Waters 150C instrument. These combined results demonstrate that during the SANS measurements termination was not a factor.

2.2. SANS measurements

SANS directly investigates in microscopic detail the scattering units with a resolution of several angstroms. It is thus the ideal tool for evaluating the structural characteristics of the intermediate-sized aggregates found in this work since their length scales R given by their radius of gyration R_g fall within the instrumental Q-range; hence R and Q are inversely related. The parameter Q, the scattering vector, is given by $4\pi \sin(\theta/2)\lambda^{-1}$ with θ the scattering angle and λ the neutron wavelength. The SANS measurements were done on the NG-7 instrument at NIST, Gaithersburg, MD. A detector setting of 12.75 m with an offset of 25 cm was used. The neutron wavelength of $\lambda = 7$ Å was used and the spread was $\Delta\lambda$ of 15%. This in turn led to an experimental Q-range of 3×10^{-3}–4×10^{-2} Å^{-1}. The scattering cross section $d\Sigma/d\Omega$ from polymers in dilute solution is given by

$$\frac{d\Sigma}{d\Omega} = \frac{\Delta\rho^2}{N_a} \frac{\Phi(1-\Phi)}{\left[\frac{1}{V_w P(Q)} + 2A_2\Phi\right]} \quad (1)$$

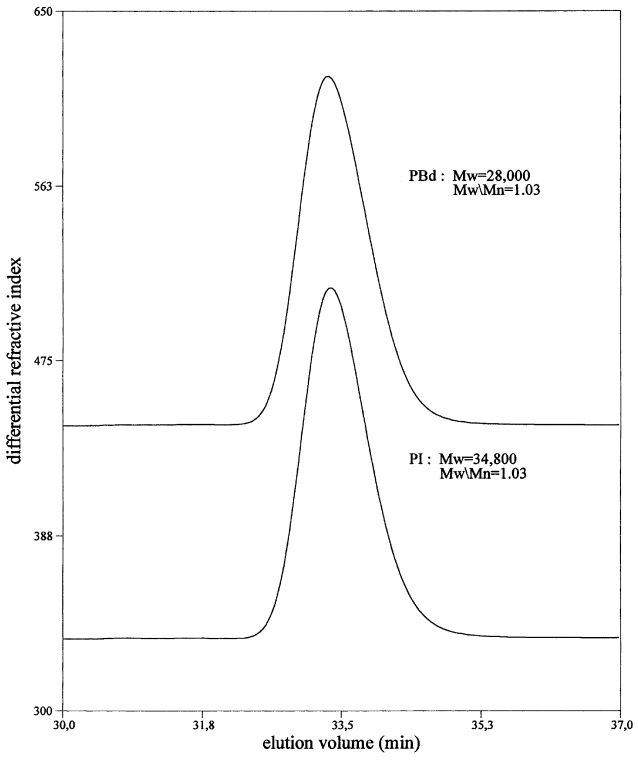

Fig. 2. SEC chromatographs of polybutadiene and polyisoprene.

Here, polymer concentration is given in terms of Φ which denotes the polymer volume fraction, $P(Q)$ the form factor of the polymer or the polymer aggregates, V_w the corresponding weight average polymer volume, A_2 the second virial coefficient, N_a the Avogadro number and Eq. (2) defines the scattering contrast

$$\Delta\rho = \left[\frac{\Sigma b_s}{V_s} - \frac{\Sigma b_{mon}}{V_{mon}} \right] \tag{2}$$

The ratio $\Sigma b_s/V_s$ is the scattering length density of the solvent while b_s denotes the scattering lengths of the atoms forming the solvent molecule and V_s is the corresponding volume. $\Sigma b_{mon}/V_{mon}$ is the corresponding quantity for the monomer unit. In general all radially averaged data were normalized to water standard. Contributions due to incoherent background and solvent scattering were subtracted from all data sets. A useful presentation of the theory and practice of SANS is available from Higgins and Benoit [24].

3. Results

Since polymer concentration increases with time the signal to noise ratio likewise increases with reaction time. An example of this is seen in Fig. 3 where the raw intensity data (corrected only for empty cell scattering) for the butadienyllithium system is displayed as a function of reaction time. In spite of the scatter at high Q the corresponding low Q data is seen to increase as Q is diminished. This scattering behavior is caused by the presence of species with larger length scales than the aggregates assayed in the mid-Q regime.

Following the start of the polymerization event the system can be considered to contain two types of monomers: (i) those incorporated into the growing chains (passive) and (ii) those awaiting reaction (active). From mass conservation the number densities N_p and N_a are related by $N_p(t) + N_a(t) = N_0$, with the total monomer number density of $N_0 = c_c N_L/M_m$. Here c_c is the given total monomer concentration in g/cm^3, M_m the monomer

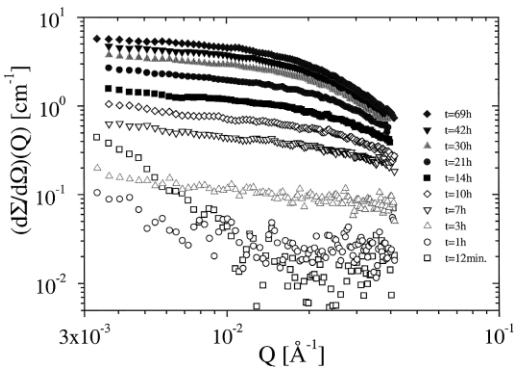

Fig. 3. Raw intensities of the polybutadienyllithium system as a function of time over the measured Q-range.

molecular weight in g/mol and N_L the Avogadro constant. From $N_p(t)$ and N_i (the initiator concentration in mol/cm^3) we can calculate the degree of polymerization D_p of the growing chain per head group as a function of time by $D_p(t) = N_p(t)/(N_i N_L)$ and hence $V_w(t)$ the molecular volume of the growing chain per head group in cm^3/mol

$$V_w(t) = D_p(t)\frac{M_m}{d_p} = \frac{N_p(t)}{N_i N_L}\frac{M_m}{d_p} \tag{3}$$

with d_p the polymer density in g/cm^3. The volume fraction of passive monomers as a function of t, $\Phi_p(t)$, can be calculated by

$$\Phi_p(t) = N_p(t) M_m/[d_p N_L] \tag{4}$$

Assuming that the growing chains form only star-like aggregates with a mean functionality of four, as predicted by the reaction mechanism under discussion, we can derive a quantitative relation between the scattering intensity $I(Q,t)$ and the number density of passive monomers $N_p(t)$. The scattering intensity as a function of reaction time t and scattering vector Q is given by

$$I(Q,t) = \phi_p(t) f V_w(t) P(Q,t) + \lfloor \phi_0 - \phi_p(t) \rfloor V_m. \tag{5}$$

Here $P(Q,t)$ is the polymer form factor which is the only Q-dependent variable. We have neglected the concentration dependence (the second virial coefficient) of $I(Q,t)$, along with the monomer form factor, $P_m(Q)$, which is one in the Q-range under consideration. Eq. (5) can be reformulated to yield

$$I(Q,t) = N_p(t)^2 \frac{M_m^2}{N_i N_L^2 d_p^2} f P(Q,t) - N_p(t)\frac{M_m^2}{N_L d_p d_m} + \frac{c_0 M_m}{d_m^2} \tag{6}$$

Assuming a constant aggregation state, this equation contains only one time dependent unknown variable, namely $N_p(t)$. Moreover, in the limit $Q = 0$, the Q-dependence of $P(Q,t)$ vanishes and Eq. (6) reduces to a simple quadratic form from which we can calculate from the forward scattering $I(Q=0,t)$ the number density of passive monomers as a function of time by

$$N_p(t) = \frac{(1/2 N_i M_m + 1/2\sqrt{N_i^2 M_m^2 - 4 c_0 f M_m N_i + 4 I(Q=0,t) f N_i \rho_m^2})\rho_p N_L}{f \rho_m M_m} \tag{7}$$

In detail, we performed the following analysis steps for extracting the forward scattering $(I, Q = 0, t)$ from our data. After correction for background and solvent scattering $I(Q,t)$ was fitted by a simple Guinier approach, $I(Q,t) = I(Q=0,t)\exp(-Q^2 R_g(t)^2/3)$. We found that our data can de described reasonably well by this approach at all stages of the polymerization. In this way we obtained two time-dependent parameters, namely $I(Q=0,t)$ and $R_g(t)$ and

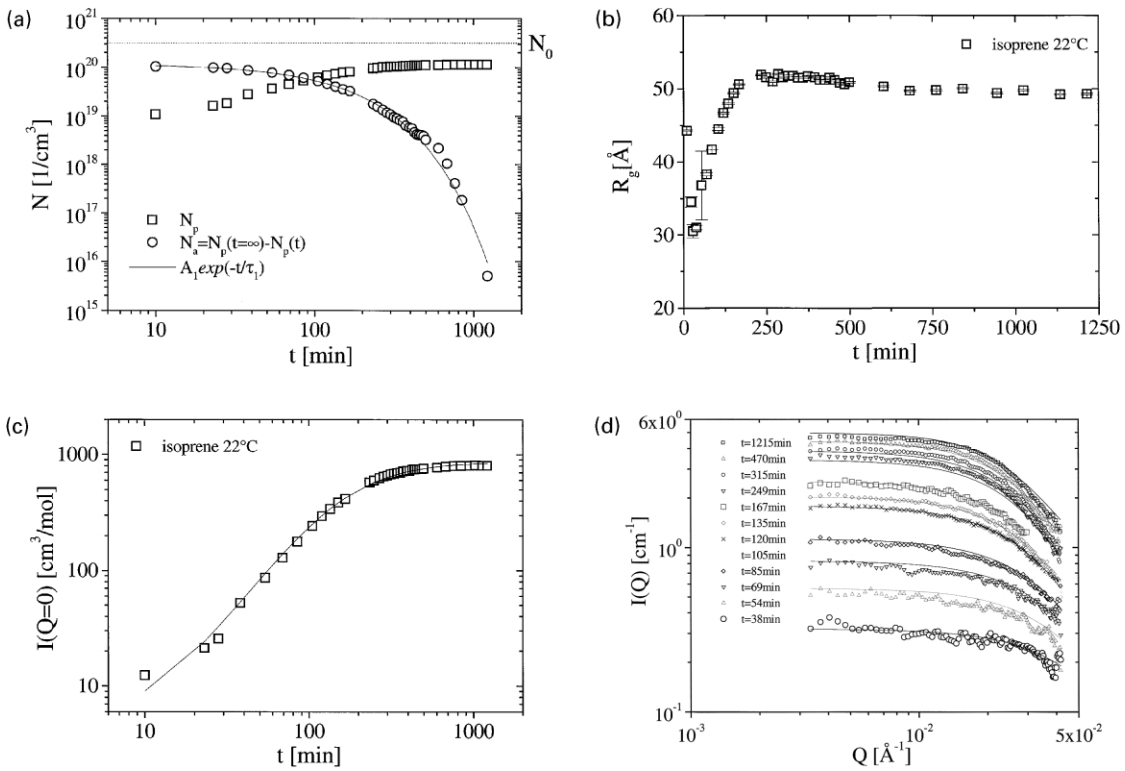

Fig. 4. (a) Conversion as a function of time for the isoprenyllithium system as a function of time. (b) Corresponding R_g as a function of time. (c) Forward scattering $I(Q=0)$ vs. reaction time for isoprene polymerization. Solid line: calculated intensity according to Eq. (9); see text. (d) $I(Q)$ vs. scattering vector Q as a function of reaction time for isoprene polymerization.

finally using Eq. (7) we can evaluate $N_p(t)$. The results of this evaluation are shown in Fig. 4(a) for isoprene.

Two points are obvious: (i) $N_p(t=\infty)$ does not reach the total monomer number density N_0 as expected. Thus neglecting the second virial coeffecient is unacceptable. (ii) However, in calculating $N_a(t) = N_p(t=\infty) - N_p(t)$ we found that $N_a(t)$ follows approximately an exponential decay, which verifies the well known first order kinetics in monomer concentration. Eq. (8) quantifies this behavior for the isoprene system

$$N_a = A_1\, e^{-t/\tau_1} \tag{8}$$

where $A_1 = 1.15 \times 10^{20}$ ($\pm 2.0 \times 10^{18}$) and the time constant, τ_1, is 129.0 (± 2.5) min obtained from best fit to the data. We note the deviations from the exponential decay at the end of the polymerization. Fig. 4(b) shows the time dependence of R_g obtained from the Guinier fit where the following can be observed: (i) An *approximate* value for R_g of 45 Å is found after the start of the reaction. It should be noted that this value is merely an approximation is based on the existing length scales of the aggregates present. (ii) A steep decrease in the very beginning of the polymerization, (iii) a subsequent increase to a maximum at ~250 min, and (iv) a slight decrease with a final leveling in the very end of the polymerization. Whereas points (i) and (ii) might indicate the presence of large aggregates already at the reaction start (but one also has to take into account the large error bars due to the low scattering intensity), points (iii) and (iv) are linked to concentration effects: We note that all values of R_g are smaller than that obtained for the terminated chain, $R_{g,term} = 71$ Å using Eq. (1) with the Debye form factor, see Table 2. This mainly arises from chain interactions. The corresponding R_g of the terminated chain obtained from the Guinier fit is ~40 Å. Calculating from this the radius of gyration of the tetramer ($f = 4$) by using the following relation $R_g = \sqrt{(3f-2)/f}R_{g,arm} = \sqrt{2.5}R_{g,arm}$ (valid for Gaussian star polymers [25]), we get a value of ~63 Å, also larger than the data shown in Fig. 4(b).

Thus, for a more quantitative analysis taking the concentration effects into account is crucial, in particular at late stages of polymerization, where both N_p and M_w are large. Countercurrent is the effect of the virial coefficient A_2. Typically a decreasing A_2 with increasing molecular weight is found, which is described by an empirical power law $A_2 \sim M_w^{-\alpha}$. For example, this exponent is -0.232 for poly(isoprene) in cyclohexane [26]. This is the limiting value for high molecular weights whereas we are on the low molecular weight side. Renormalization group theory predicts that A_2 approaches a constant value for small M_w [27]. Combining the M_w and the time-independent second virial coeffcient with the observed first order kinetics (the exponential decay of N_a) with time, we can now try to

describe our data by putting Eqs. (3), (4) and (8) into Eq. (1)

$$I(Q=0) = \frac{N_p M_m}{\rho_p N_l \left(\frac{N_i N_p \rho_p}{f N_p M_m} + \frac{2A_2 N_p M_m}{\rho_p N_l} \right) + \frac{\left(\frac{c_0}{\rho_p} + \frac{N_p M_m}{\rho_p N_l} \right) M_m}{\rho_m}} \quad (9)$$

The appropriate quantity is the forward scattering $I(Q=0,t)$, i.e. assuming $P(Q)=1$, which is affected by A_2 and the result of the fit is shown in Fig. 4(c). With this second parameter A_2 we can now describe the forward scattering during all stages of the polymerization and arrive at the correct value for $N_p(t=\infty)$. We obtained the following results: $\tau_1 = 397 \pm 5$ min and $A_2 = 5.99(\pm 0.6) \times 10^{-4}$ cm^3 mol/g^2. The characteristic time τ_1 of the exponential decay severely changes using this approach compared to application of Eq. (7). The second virial coeffecient (A_2) is within error bars the same than that for the terminated chain, $A_{2,\mathrm{term}} = 7.40(\pm 0.3) \times 10^{-4}$ cm^3 mol/g^2.

In the last step of our analysis we try to describe the complete Q-dependence by using the Benoit form factor of a Gaussian star polymer [22]. The arms of the star polymer are the growing chains, for which we assume the following power law relation between R_g and $M_w/R_g = 0.385 M_w^{0.5}$. The exponent 0.5 arises from the low molecular weights under consideration [26] and the prefactor is adjusted to give the value of 71.8 Å for the terminated chain. The result of this calculation using the τ_1 and A_2 found earlier is shown in Fig. 4(d) together with the experimental. The agreement between calculation and experiment is striking. A complex data set of more than 4000 t- and Q-dependent points can be adequately described by one parameter, the characteristic time τ_1 of the monomer concentration decay. This behavior of $R_g(t)$ shows the complex aggregation behavior of the living chains. The approach given above is not viable for the butadiene case in view of the indicated presence of large-scale objects in coexistence with the star aggregates at the completion of the polymerization.

Fig. 5 shows, in a linear fashion, the SANS scattering profile for the butadienyllithium head group as a function of time. The main message is contained in the low Q data where the raw intensity is seen to decrease with increasing reaction time. In a corresponding fashion the mid-Q regime registers a small increase in intensity with time. This demonstrates that the large-scale structures disintegrate as chain length increases. This is in accord with the findings of Makowski and Lynn[2] for room temperature oligomeric butadienyllithium in the neat state. Also note that the scattering from the initiator solution (where the aggregation state of *sec*-BuLi is 4) is independent of Q as was that from the monomer solutions. Thus, the scattering at low Q in Fig. 5 is the signature of species formed immediately after the completion of the initiation event. The presence of this enhanced scattering from a very low volume fraction of polymer is an indication that the aggregated structures formed are quite large.

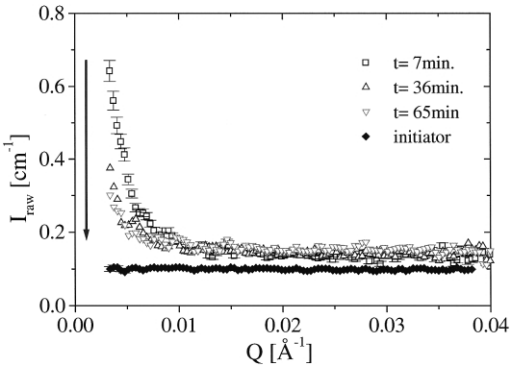

Fig. 5. Raw intensities of low conversion data as a function of Q for butadienyllithium.

The corresponding isoprenyllithium system shows somewhat different behavior as a function of reaction time, see Fig. 6. In essence, the low Q data (>0.01 Å^{-1}) shows, in a parallel fashion, the presence of the aggregates with larger length scales than are seen in the region of larger Q. Like the butadiene system these structures melt as the propagation reaction proceeds. The failure of the higher Q-range intensities to coalesce as seen in Fig. 5 for the butadiene-based system is due to the fact that isoprene polymerizes at a faster rate than butadiene. This is highlighted by the data in Fig. 7 where the scattering data (corrected for background) are shown for the two systems at approximately the same interval into the propagation reaction. This is further amplified by the contrast shown in Fig. 8 for longer reaction times.

We cannot assign an aggregation number to these large-scale aggregates since we have only captured a fraction of the low Q scattering profile. A complete profile covering the larger length scales requires the experimental capacity to enter the Q-range of $<10^{-3}$ Å, which is typical for light scattering. This will be possible with the new SANS KWS-3 beamline at the Ella FRJ-2 Jülich research reactor.

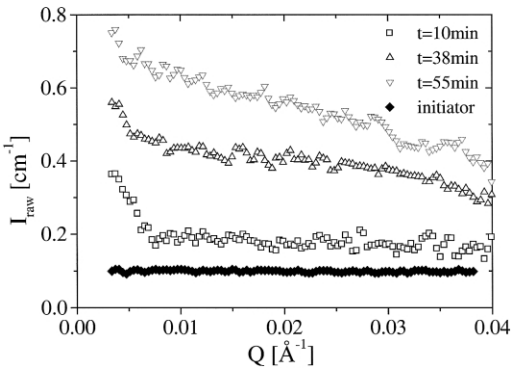

Fig. 6. Raw intensities of intermediate conversion data for polyisoprenyllithium.

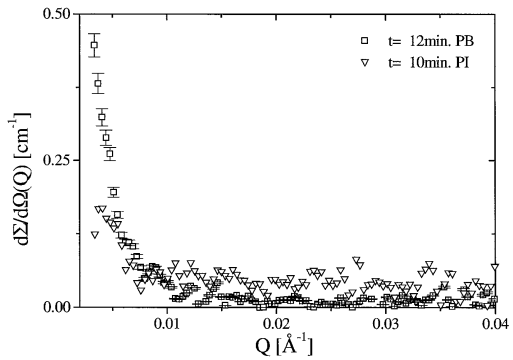

Fig. 7. Corrected scattering at low conversions for polyisoprenyllithium and for butadienyllithium.

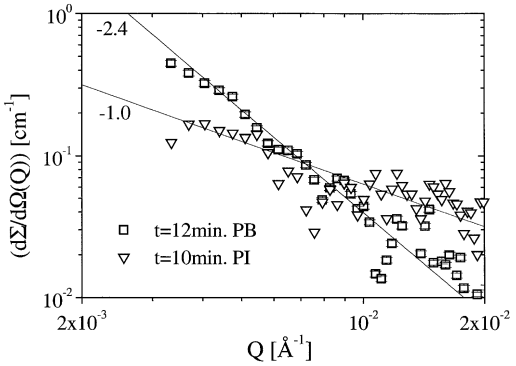

Fig. 9. Log–log plot of corrected scattering at low conversions for polyisoprenyllithium and for butadienyllithium.

Nonetheless, the low-Q data in hand (Fig. 7) allows some conclusions regarding the architecture of these aggregates. These data, the SANS macroscopic scattering cross sections $d\Sigma/d\Omega$ vs. the momentum transfer Q, are reproduced in Fig. 9 in the double logarithmic format. Neither family of aggregates shows Debye-chain behavior, i.e. the zero gradient in the mid to low-Q-range; see the polyisoprene scattering profiles obtained at complete conversion in Fig. 10. If present this would be strong evidence for the presence of only star-shaped aggregates.

The characteristic feature of both headgroups is the appearance of two power laws according to

$$\frac{d\Sigma}{d\Omega} = (Q) \propto Q^{-\beta} \tag{10}$$

with an exponent characteristic for certain arrangements of the aggregation structures. At large Q one finds for the terminated polyisoprene and polybutadiene an exponent of $\beta \cong 1.67$ indicative of excluded volume interaction between the monomers of single chains in a good solvent. There the chain conformation follows a self-avoiding random walk with a fractal dimension $D = \nu^{-1}$ where ν is the Flory exponent of 3/5. The increase in the intensity at lower Q (see Figs. 5–7) is caused by polymer aggregates other than star-shaped. The polyisoprenyllithium system (Fig. 9) with a gradient of approximately -1 is indicative of the presence of one-dimensional species. Needle or rod-like structures will give rise to such scattering behavior in the low-Q region [22]. Conversely, the butadienyllithium headgroup (Fig. 9) yields a gradient of about -2.4. This behavior is the signal of large-scale fractal structures. Similar findings were reported previously [3]. In general if we consider a fractal object of fractal dimension D its mass M scales with its size R according to $M \propto R^D$. Thus the scattering cross-section for such an object takes the form of Eq. (4) keeping in mind that $\beta \equiv D$. Thus a power law regime in Q with an exponent between 2 and 3 relates to a fractal object of dimension D. SAXS and SANS based evidence is available [28] for the formation of similar large-scale structures formed by the aggregation of monocarboxylic chains.

The scattering profiles for the structures observed at complete conversions are shown in Figs. 10 and 11. Fig. 10 shows the scattering profile of polyisoprenyllithium wherein the use of the Benoit star form factor leads to the mean aggregation state of four. The data of Fig. 11 yields a similar, but not identical state of play for the butadienyllithium aggregates. Here, the mean aggregation state is found to be about 8.6. This value is well removed from the limiting value of four required by the current mechanism. An additional observation is that, even at complete conversion, an indication exists in the lowest Q regime that some large-scale structures (relative to the star with $f = 8.4$) are present. Bywater has questioned [29] the

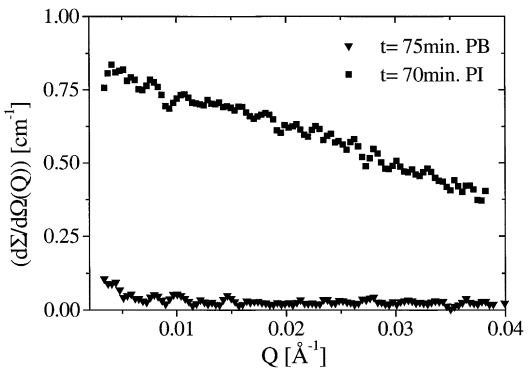

Fig. 8. Corrected scattering at intermediate conversions for polyisoprenyllithium and for butadienyllithium.

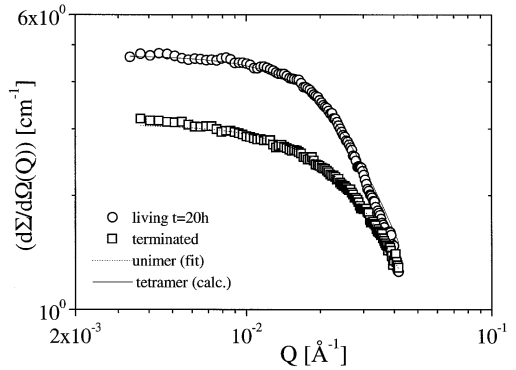

Fig. 10. Corrected scattering of polyisoprenyllithium and terminated polyisoprene as a function of Q; complete conversion.

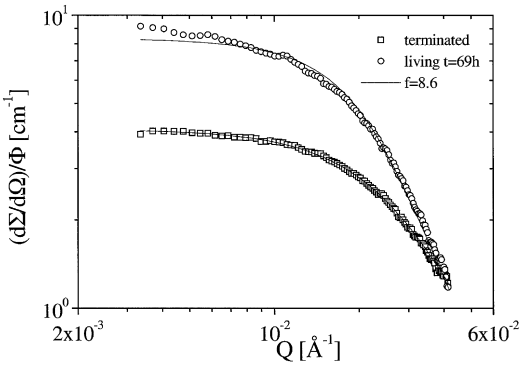

Fig. 11. Corrected scattering of polybutadienyllithium and terminated polybutadiene as a function of Q; complete conversion.

existence of non-star shaped structures in these systems. It is sufficient to state that he provides no new experimental data to support his view of 'tetramers only' in alkane based systems. The data of Makowski and Lynn [19] also contradicts his assessment.

4. Final discussion

The foregoing has presented additional evidence for the existence of diverse aggregate architectures and functionalities (where the limiting lower value is the dimer [19,30]) that are not countenanced by the long accepted textbook mechanism [15–18]. An important ramification of these findings is the question of aggregate reactivity. This is unacceptable to the mechanism in question. Measured and calculated values indicate that these allylic headgroups have dimeric aggregation enthalpies of ca. 40 kcal/mol [30].[3] These values preclude the presence of singlet headgroup concentrations needed to carry out the observed diene polymerization reactions. Calculations are available which support this conclusion [31]. This in turn requires that aggregation does not eliminate head-group reactivity. This notion was endorsed in 1966 by Brown [32], Makowski and Lynn [19] and latter by others [33,34]. It has been shown [35,36] that ethylene oxide and butadiene vapor will rapidly react with freeze-dried polystyryllithium powder at room temperature. The sub-glass transition status of the polystyrene chain precludes headgroup dissociation. Thus, the reactivity of aggregated active centers is demonstrated.

An interesting and valuable observation [37,38] is the demonstration that polymer chain length can influence the polymerization rates (and hence the apparent kinetic order) of butadiene (cyclohexane) and isoprene (cyclohexane and benzene) at 20 °C. About 40–50% increase in measured rates was found [37] when the rates obtained from low molecular weight chains ($<2\times10^3$ g/mol) were compared to the rates obtained from systems where the limiting molecular weight was ca. 2×10^4 g/mol or larger. The headgroup concentrations were held constant for each 'matched pair' of comparative runs and covered the headgroup concentration range of 1.2×10^{-3}–1×10^{-4} M. These findings were explained in terms of an increase in the equilibrium constant for the tetramer to dimer event; Eq. (11)

$$(\mathrm{PLi})_4 \leftrightarrows 2(PLi)_2 \tag{11}$$

The perceived enhancement of the dimer population was credited [37] to excluded volume effects which were believed to come into play as star arm length increased. This argument is incorrect as shown by the observation that large-scale structures exist (this work, Ref. [3]) when chain length is relatively small. Thus, the 'tetramers only' notional of Eq. (11) [15–18] is invalid.

Hence, headgroups in the aggregates are reactive and that reactivity seemingly can increase as the extent of aggregation decreases. The larger propagation reactivity exhibited by the higher molecular weight chains demonstrates that the headgroups in the large-scale structures have restricted reactivities relative to those within smaller functionality aggregates. Thus, chain length can influence the observed rate of polymerization [37,38]. These observations contradict the assumption [15–18] that aggregation states directly reflect kinetic orders.

[3] See Ref. [9] and references contained therein.

References

[1] Fetters LJ, Balsara N, Huang JS, Jeon HS, Almdal K, Lin MY. Macromolecules 1995;28:4996.
[2] Stellbrink J, Willner L, Jucknischke O, Richter D, Lindner P, Fetters LJ, Huang JS. Macromolecules 1998;31:4189.
[3] Stellbrink J, Willner L, Richter D, Lindner P, Fetters L, Huang JS. Macromolecules 1999;32:5321.
[4] Fetters LJ, Huang JS, Sung J, Stellbrink J, Richter D, Lindner P. In: Quirk RP, editor. ACS symposium series, vol. 696. Washington: ACS; 1996. p. 36.
[5] Davidson NS, Fetters LJ, Funk WG, Graessley WW, Hadjichristidis N. Macromolecules 1988;21:112.
[6] Fetters LJ, Graessley WW, Hadjichristidis N, Kiss AD, Pearson DS, Younghouse LB. Macromolecules 1988;21:1644.
[7] Hadjichristidis N, Pispas S, Pitsikalis M. Prog Polym Sci 1999;24:875.
[8] Halperin A, Tirrell M, Lodge TE. Adv Polym Sci 1992;100:31.
[9] Frischknecht A, Milner ST. J Chem Phys 2001;114:1032.
[10] Witen TA, Pincus PA, Cates ME. Eur Phys Lett 1986;2:137.
[11] Willner L, Jucknischke O, Richter D, Farago B, Fetters LJ, Huang JS. Eur Phys Lett 1992;19:297.
[12] Richter D, Jucknischki O, Willner L, Fetters LJ, Lin M, Huang JS, Roovers J, Toporowski PM, Zhou LL. J de Phys I Colloque C8 1993;3:3.
[13] Willner L, Jucknischke O, Richter D, Roovers J, Zhou LL, Toporowski PM, Fetters LJ, Huang JS, Lin MY, Hadjichristidis N. Macromolecules 1994;27:3821.
[14] Likos CN, Lowen H, Poppe A, Willner L, Roovers J, Cubitt B, Richter D. Phys Rev E 1998;58:6299.
[15] Szwarc M. Adv Polym Sci 1983;49:1.
[16] Szwarc M, Van Beylen M. Ionic polymerization and living polymers. New York: Chapman & Hall; 1993.

[17] Van Beylen M, Bywater S, Smets G, Szwarc M, Worsfold DJ. Adv Polym Sci 1988;86:87.
[18] Duda A, Penczek S. Macromolecules 1994;27:4876.
[19] Makowski H, Lynn MJ. Macromol Sci 1966;1:443.
[20] Morton M, Fetters LJ. Rubber Chem Technol 1975;48:359.
[21] Bach RO, Kamienski CW, Ellested RB. Encycl Chem Technol 1967; 1:529.
[22] Sinn H, Lundborg C, Onsager OT. Makromol Chem 1964;70:222.
[23] Gebert W, Hinz J, Sinn H. Makromol Chem 1971;144:97.
[24] Higgins JS, Benoit H. Polymers and neutron scattering. Oxford: Clarendon Press; 1994.
[25] Grest GS, Fetters LJ, Huang JS, Richter D. In: Prigogine I, Rice SA, editors. Advanced chemical physics XCIV. New York: Wiley; 1996. p. 67.
[26] Fetters LJ, Hadjichristidis N, Lindner JS, Mays JW. Phys Chem Ref Data 1994;23:619.
[27] Elias HG. Makromolekule. Hüthig Wepf: Basel; 1990. p. 17.
[28] Jalal N, Duplessix R. J Phys Fr 1988;49:1775.
[29] Bywater S. Macromolecules 1998;31:6011.
[30] Morton M, Fetters LJ. J Polym Sci, Part A 1964;2:3311.
[31] Szwarc M. Polym Sci, Polym Lett 1980;18:493.
[32] Brown TL. J Organomet Chem 1966;5:191.
[33] Sapse A-M, Jain DC, Raghavachari K. In: Sapse A-M, Schleyer PvR, editors. Lithium chemistry: a theoretical and experimental overview. New York: Wiley; 1995.
[34] Smart JB, Hogan R, Scheer PA, Emerson MT, Oliver JP. J Organomet Chem 1974;64:1.
[35] Quirk RP, Chen WC. Makromol Chem 1982;183:2071.
[36] Young RN, Fetters LJ, Huang JS, Krishnamoorthi R. Polym Int 1994; 33:217.
[37] Bywater S, Worsfold DJ. In: Hogen-Esch TE, Smid J, editors. Recent advances in anionic polymerization. New York: Elsevier; 1987. p. 109.
[38] Mardini AE, Favier JC, Hemery P, Sigwalt P. Makromol Chem Rapid Commun 1990;11:329.